Mapping GPS-derived ionospheric Total Electron Content over Southern Africa during different epochs of solar cycle 23

D.M. Moeketsi, W.L. Combrinck, L.A. McKinnell and M. Fedrizz

Abstract

The Southern African Development Community and the International Global Navigation Satellite Systems Service (GNSS) network of dual frequency Global Positioning System (GPS) receivers provide an opportunity to determine Total Electron Content (TEC) over Southern Africa by taking advantage of the dispersive nature of the ionospheric medium. For this task, the University of New Brunswick (UNB) ionospheric modelling technique which applies a spatial linear approximation of the vertical TEC above each station using stochastic parameters in Kalman filter estimation, primed with data from the Southern Africa GPS network, was used for mapping TEC at South African locations during selected days and hours of different epochs of solar cycle 23. Significant enhancements in the TEC value and features, which could be associated with frequent solar events, are evident around a day of extreme solar maximum. These observations are discussed and further investigated by analyzing the GOES 8 and 10 satellites X-ray flux (0.1–0.8 nm) and SOHO Solar EUV Monitor (26.0–34.0 nm) higher resolution data. Comparison of these physical quantities reveals that for each X-ray flare observed, there is an associated EUV flare event. The latter phenomenon causes photoionisation in the daytime ionosphere which results in significant TEC enhancement. The daytime UNB TEC compared with the International Reference Ionosphere (IRI) 2001 predicted TEC found both models to show a good agreement.

1. Introduction

The current trend in ionospheric physics research has proven that the dual frequency (L1 = 1575.42 MHz and L2 = 1227.60 MHz) signals transmitted by the Global Navigation Satellite Systems (GNSS), and received by the network of Global Positioning System (GPS) receivers distributed worldwide provide a unique opportunity to determine the high resolution spatial and temporal ionospheric Total Electron Content (TEC) at regional and global level (e.g. Klobuchar, 1991, Komjathy and Langley, 1996, Jakowski, 1996, Komjathy, 1997 and Mannucci et al., 1998). This is possible due to the dispersive nature of the ionospheric medium. Electromagnetic waves, such as GPS signals, experience time delays when traversing the ionosphere (Ratcliffe, 1959). The delay of the GPS broadcasting signals is directly proportional to the integrated free-electron density (TEC) along the signal path from the broadcasting position in space to the receiver on Earth. The magnitude of TEC is highly variable and depends on several factors such as local time, geographical location, season, and solar activity cycle (e.g. Jakowski, 1996, Jakowski et al., 1999, Jakowski et al., 2002, Immel et al., 2003, Tsurutani et al., 2004, Skoug et al., 2004, Jee et al., 2005, Mannucci et al., 2005 and Fedrizzi et al., 2001). Recent studies (Jakowski et al., 2001 and Jakowski et al., 2002) illustrate that TEC monitoring using the GNSS network, can contribute to space weather monitoring. The unit for TEC used in this work is TECU where 1 TECU = 10^{16} electrons/m^2.

This paper presents an attempt to study the solar cycle variations of TEC observed over the southern African region with the aid of the University of New Brunswick (UNB) ionospheric modeling technique (Komjathy, 1997). Komjathy (1997)

developed and applied this model for mapping the global and regional ionospheric TEC using the worldwide GPS network with stations mainly densely distributed in the northern hemisphere. This model was developed to provide ionospheric corrections to single frequency users (Komjathy et al., 1998). Most recently, Fedrizzi et al. (2005) also used the same model to study TEC variability associated with geomagnetic storm activity over locations in the South American Sector. The current data available from the Hartebeeshoek Radio Astronomy Observatory (HartRAO) International GNSS Service and the Chief Directorate Surveys and Mapping (CDSM) Trignet network of dual frequency GPS receivers distributed over southern Africa make this study possible (Cilliers et al., 2003 and Combrink et al., 2004).

For the purpose of this work, the monthly averaged sunspot number was used as a proxy for solar activity cycle 23 as shown in Fig. 1. From these monthly averaged values, it is well established that the Sun has a quasi-periodic ~11 year activity cycle (e.g., Smith and Marsden, 2003). Approximately every 11 years the Sun moves through a period of fewer and smaller sunspots, which is called 'solar minimum' followed by a period of larger and more sunspots which is called 'solar maximum'. Different epochs of the solar cycle were selected based on the availability of GPS data within southern Africa as follows: epoch "(a)" the moderate solar activity conditions around 1998 (left shaded band) during the ascending phase of the solar cycle; epoch "(b)" the extreme solar maximum conditions around 2001 (middle shaded band); and epoch "(c)" the moderate solar activity conditions around 2004 (right shaded band) during the descending phase of the solar cycle 23. Subsequent effects of these different epochs on TEC maps over southern Africa are discussed. TEC observations around a selected day and hour during an extreme solar maximum period display interesting features which could be associated with frequent solar activity events. These observations are further investigated by analyzing the GOES 8 X-ray flux (0.1–0.8 nm) data and the Solar and Heliospheric Observatory (SOHO): Charge, Element and Isotope Analysis/Solar Extreme Ultraviolet Monitor (CELIAS/SEM) 26.0–34.0 nm higher resolution data. The latter instrument's detailed description can be obtained from Hovestadt et al., 1995, Judge, 1998, Judge et al., 2001 and Judge et al., 2002. The daytime TEC computed with the UNB model are comprehensively compared with TEC values computed with the recent version of the International Reference Ionosphere (IRI) 2001 model (Bilitza, 2001).

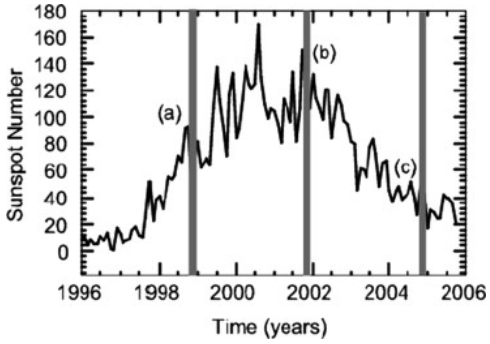

Fig. 1. Monthly averaged sunspot number for solar cycle 23. The shaded regions depict selected day 345 at 14:00 UT for different epochs of solar cycle 23. Epoch "(a)" represents intermediate solar activity conditions during the ascending phase; "(b)" represents extreme solar maximum conditions during the peak; and "(c)" represents the descending phase of the solar cycle.

2. UNB ionospheric modelling technique

The UNB ionospheric modelling technique uses the single-layer ionospheric (shell) model to compute TEC from dual frequency GPS receivers, according to the following observation equation (Komjathy, 1997):

$$I_r^s(t_k) = M(e_r^s)[a_{0,r}(t_k) + a_{1,r}(t_k)\mathrm{d}\lambda_r + a_{2,r}(t_k)\mathrm{d}\varphi_r] + b_r + b^s \quad (1)$$

where $I_r^s(t_k)$ represent the line-of-sight L1–L2 phase-leveled measurements obtained by receiver *r* and observing satellite s at epoch t_k. $M(e_r^s)$ is the mapping function, e_r^s represents the satellite elevation angle, $a_{0,r}$, $a_{1,r}$, and $a_{2,r}$ are stochastic parameters for spatial linear approximation of TEC to be estimated for receiver r and assuming a first-order Gauss-Markov stochastic process (Gail et al., 1993). Furthermore, $\mathrm{d}\lambda_r = \lambda_r - \lambda_0$ is the difference between a sub-ionospheric point and the mean longitude of the Sun, $\mathrm{d}\varphi_r = \varphi_r - \varphi_0$ is the difference between the geomagnetic latitude of the sub-ionospheric point and the geomagnetic latitude of the station, b_r and b^s refer to the receiver and satellite instrumental biases, respectively. For further information on how these biases are estimated, see Komjathy (1997).

The PhaseEdit version 2.2 automatic data editing program was used to detect bad points and cycle slips, as well as repair the cycle slips and adjust phase ambiguities using the undifferenced GPS data. The program takes advantage of the high precision dual frequency pseudorange measurements to adjust L1 and L2 by an integer number of cycles to agree with the pseudorange measurements (Fedrizzi et al., 2005). The elevation cutoff angle was set to 10°.

In this work the standard geometric mapping function

$$M(e_r^s) = \left[1 - \frac{r_E \cos^2 e_r^s}{(r_E + h)^2}\right]^{-\frac{1}{2}} \quad (2)$$

is used (Mannucci et al., 1993). Here, r_E is the mean radius of the Earth and *h* is the mean value for the assumed height of the thin spherical ionospheric shell, located at a height of 400 km slightly higher than the average height of the maximum electron density (Komjathy, 1997). Eq. (2) computes the secant of the zenith angle of the signal geometry ray path at the ionospheric pierce point and projects the line-of-sight measurements to the vertical of the sub-ionospheric point. It should be noted that recent studies of comparison of techniques for mapping TEC reported an improvement in accuracy of mapping TEC compared with the thin shell approach (Meggs et al., 2004 and Meggs and Mitchell, 2006).

Because of the ionospheric dependence on solar radiation and the geomagnetic field, a solar-geomagnetic reference frame is used to compute the TEC at each grid point. TEC values change much more slowly in this reference frame compared to an Earth-fixed one. The ionospheric model was evaluated for the four closest stations to a grid node at which a TEC value is computed. Subsequently, the inverse-distance-squared weighted averages of the individual TEC data values for the four stations were computed. The closer a particular grid node is to a GPS station, the more weight is placed on the TEC values computed by evaluating the ionospheric model describing the temporal and spatial variation of

the ionosphere above the particular station. The ionospheric TEC maps are produced using a 5-degree grid spacing. Each fifteen minutes map reflects the observations obtained from 7.5 min before to 7.5 min after the respective quarter hour (Fedrizzi et al., 2005).

3. Observations and data analysis

The data sampled at 30 s from 11 International GNSS and 10 Southern African Development Community (SADC) dual frequency GPS receivers, distributed within southern Africa, were used in this study as an input to the UNB code described in Section 2. The station's geographical coordinates and geomagnetic latitudes are listed in Table 1 and illustrated on the southern Africa map shown in Fig. 2. The International GNSS data used is obtained from ftp://lox.ucsd.edu/pub/rinex and can also be obtained from the HartRAO data server ftp://geoid.hartrao.ac.za, while the CDSM Trignet data were obtained from ftp://www.trignet.co.za. The quality of the GPS data was checked for all stations using the Translate/Edit/Quality Check (TEQC) software. The software module "EditObs" developed locally (Ngcobo et al., 2005) was used to edit the Receiver Independent Exchange format (RINEX) GPS observation file and create a new

RINEX file, which contains GPS observables used by UNB code during the computations. The HRAO station was chosen as a reference station based on its central location and good quality data available for the period of interest to this study. Furthermore, the sunspot number and disturbance storm time index (DST) data used in this study as proxies for solar cycle and geomagnetic activity were obtained from http://www.spaceweather.com and http://swdcwww.kugi.kyoto-u.ac.jp. The SOHO CELIAS/SEM and GOES X-ray data used in the analysis were obtained from http://www.usc.edu/dept/space_science/semdata and http://goes.ngdc.noaa.gov/data respectively.

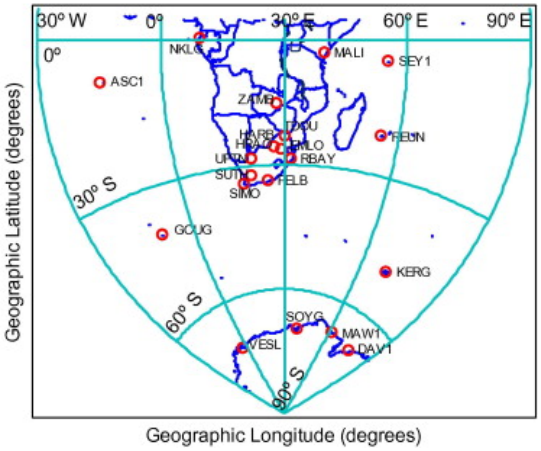

Fig. 2. Southern African geographical map showing the distribution of the ground based International GNSS and SADC network of dual frequency GPS stations (red cycles) used in this study. (For interpretation of the references to colour in this figure legend, the reader is referred to the web version of this article.)

Table 1
Geographic coordinates and geomagnetic latitudes of international GNSS and SADC GPS stations used in this study

	Geographical latitude (°)	Geographical longitude (°)	Geomagnetic latitude (°)
International GNSS stations			
SOYG	−69.58	39.58	−70.88
VESL	−71.67	357.16	−66.06
GOUG	−40.38	350.13	−35.00
MALI	−2.99	40.19	−6.77
DAV1	−68.58	77.97	−74.60
ASC1	−7.95	345.59	−2.35
NKLG	0.35	9.67	1.86
MAW1	−67.60	62.87	−73.22
SEY1	−4.67	55.48	−10.81
REUN	−21.21	55.57	−27.18
KERG	−49.35	70.23	−56.93
SADC GPS and GNSS stations			
HRAO	−25.89	27.69	−27.13
HARB	−25.89	27.71	−27.13
RBAY	−28.80	32.08	−30.76
SUTH	−32.38	20.81	−32.26
S121	−25.74	28.22	−27.09
ZAMB	−15.43	28.31	−16.97
UPTN	−28.41	21.26	−28.46
EMLO	−26.50	29.50	−28.05
SIMO	−34.19	18.44	−33.61
TDOU	−23.08	30.38	−24.85
PELB	−33.98	25.61	−34.68

Results and discussion

4.1. Mapping TEC during different epochs of solar cycle 23

A common day and time (Day 345, 14: 00 UT) was selected during different epochs of solar cycle 23. The epochs selected are indicated as (a), (b) and (c) in Fig. 1 and refer to:

“(a)” the moderate solar activity conditions around 1998 during the ascending phase of the solar cycle;

“(b)” the extreme solar maximum conditions around 2001; and

“(c)” the moderate solar activity conditions around 2004 during the descending phase of the solar cycle as discussed in Section 1 for the purpose of this study.

Fig. 3(a)–(c) display the TEC maps computed with the UNB model over South Africa for the different selected epochs of solar cycle 23. Evidently, TEC values computed for epochs “(a)” and “(c)” are comparable and increase towards low latitudes as expected. Furthermore, TEC values computed for epoch “(b)” are significantly higher than for epochs “(a)” and “(c)”, respectively. These observations are possible because of the high rate of production of solar EUV and X-ray radiation during the period of maximum solar activity conditions, which causes significant photoionisation within the daytime ionosphere resulting in relatively high TEC values compared to moderate and low solar activity. Of particular interest on the TEC map for epoch “(b)” is the double peak display with enhanced TEC values near mid-latitudes comparable with values observed towards the lower latitudes. An attempt was undertaken to investigate possible causes of this midlatitude enhanced TEC peak anomaly by analyzing the DST index shown in Fig. 4(a). It is evident from this approach that day 345 of the year 2001 was geomagnetically quiet with DST >−20 nT, which implies that the observed TEC anomaly near mid-latitudes is not associated with geomagnetic activity. It should be noted that DST for day 345, in 1998 and 2004 was also found to be >−42 nT.

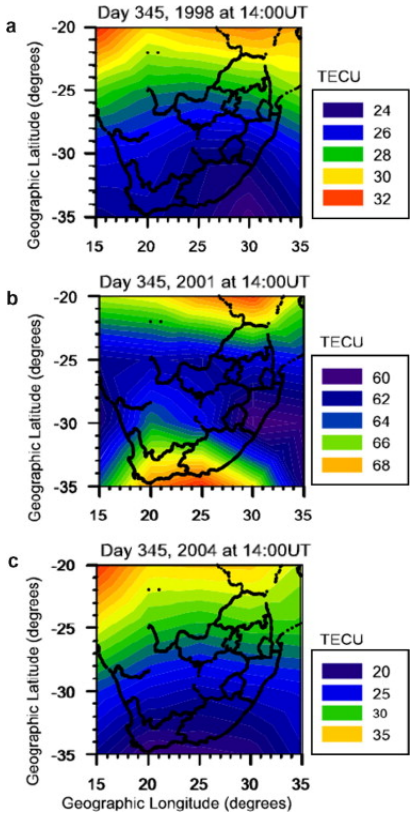

Fig. 3. South Africa TEC maps computed using the UNB code for day 345 at 14:00 UT for the different epochs of solar cycle 23 described in Section 1 and depicted in Fig. 1.

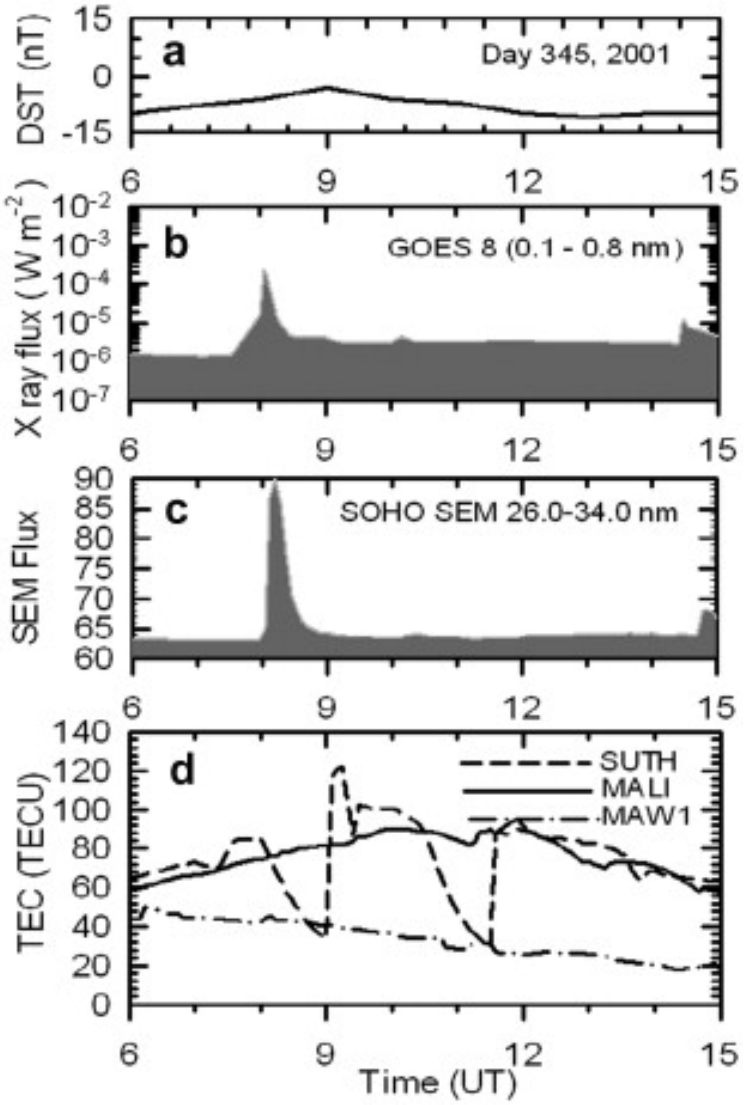

Fig. 4. The day 345, 2001 solar X28 flare. The different panels show: (a) Disturbance Storm Index (DST) measurements, (b) GOES 8 five minute average X-ray fluxes on the 0.1–0.8 nm wavelengths band, (c) SOHO SEM five minute average EUV fluxes on the 26.0–34.0 nm wavelength band and (d) UNB five minute TEC observed over MALI (solid line), SUTH (dashed line), and MAW1 (dash-dot-dash line), respectively. The SEM EUV fluxes are in unit of (photons/cm^2/s × 10^9).

However, a further investigation was conducted by analyzing the five minute averaged GOES 8 satellite X-ray (0.1–0.8 nm) flux and SOHO CELIAS/SEM (26.0–340 nm) measurements for day 345, 2001 shown in Fig. 4(b) and (c), respectively. It should be noted that CELIAS/SEM 26.0–34.0 nm channel time series data has shown that this channel is not sensitive to X-rays as reported in Tsurutani et al. (2005). It became clear from this analysis that GOES 8 recorded an X-ray flare of magnitude X28 at ~8.05 UT. Interestingly, the SEM EUV instrument aboard SOHO also observed a EUV

flare event associated with the recorded X-ray flare. The X-ray fluxes show that the flare occurred at ~7:50 UT and reached a peak intensity at ~8:05 UT. The EUV flare seems to have occurred later at ~8:00 UT and reached maximum peak intensity at ~8:05. The decay phase of both flares took much longer (~45 min) to reach the inertial background before the onset of the flares.

To investigate the effects of these flares on TEC, Fig. 4(d) shows the UNB five minute averaged TEC between 6:00 UT and 15:00 UT. TEC are shown over GPS stations at low latitudes (MALI), midlatitudes (SUTH) and higher latitudes (MAW1), respectively. For the SUTH midlatitude station, a simultaneous increase in TEC was evident at the onset of the X-ray flare reaching a maximum enhancement value of ~20 TECU above the background just before the onset of the EUV flare, at which, the TEC over SUTH decreased abruptly to a minimum value of ~32 TECU around 9:00 UT and suddenly increased sharply to ~124 TECU within 20 min and decreased instantly to have a minimum value of ~28 TECU around 11:45 UT. Furthermore, TEC values suddenly increased again to reach a maximum value of ~84 TECU around 12:00 UT and decreased gradually without large variations after noon as expected. No such TEC perturbations were observed over the MALI and MAW1 GPS stations. Of interest is that the TEC values over SUTH located in the vicinity of the observed TEC peak anomaly seems to be comparable with TEC values over MALI. However, TEC values over MALI seem to be averaged compared to those observed over SUTH after the decay phase of the flares, while TEC over MAW1 remained significantly lower and gradually decreased throughout this period. Fig. 5 shows the UNB five minute averaged TEC between 6:00 UT and 18:00 UT for midlatitude GPS station HARB and S121 located not far from SUTH. Evidently, pronounced TEC variation occurs over both stations at the onset of EUV flare. TEC variation took longer (shaded period) than the duration of the flare. The ionospheric TEC response due to this flare seems to be localized, however, more data and further investigations is required to explore this possibility. The observed high sharp intensity (90×10^9 photons/cm^2/s) peak of EUV could be the cause of the ~3 h TEC variation over SUTH and the subsequent lengthy TEC variation over HARB and S121. However, the near mid-latitude peak anomaly (enhanced ionisation) on the TEC map during extreme solar maximum conditions may be due to particle precipitation from the outer radiation belt at latitude >30° South as a result of this flare. Although the latter explanation is likely, more data is required to substantiate it.

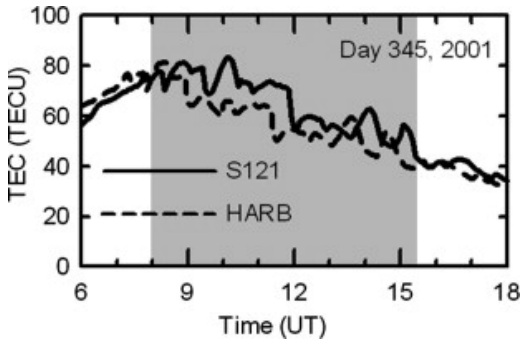

Fig. 5. The S121 (solid line) and HARB (dashed line) TEC response due to the day 345, 2001 solar X28 flare.

Earlier studies of the solar flare effects on the ionosphere have identified sudden ionospheric disturbances (Thome and Wagner, 1971, Mitra, 1974 and Donnelly, 1976). However, to further investigate the effects of flares on GPS derived TEC over southern Africa, Fig. 3(a) and (b) show the GOES 10 satellite 0.1–0.8 nm X-ray fluxes and SOHO SEM 26.0–34.0 nm fluxes observed between 10:00 UT and 13:00 UT on day 301, 2003 during the recorded X17 flare event. The global effects of this flare on ionospheric TEC derived from the worldwide GPS network were recently studied (e.g. Tsurutani et al., 2005 and Zhang and Xiao, 2005). The X-ray flux measurements show that the flare occurred at ~11:00 UT and reached a peak at ~11:10. The decay phase of the flare took much longer (~1 h 30 min) and reached the background level at ~12:40 UT. The EUV flare occurred simultaneously as the X-ray flare, but show a double peak at ~11:10 UT and at ~11:20 UT, respectively. The decay period took almost the same time as the X-ray flare. The increase in SEM data after ~12:30 UT is not EUV flux, but it could be a contribution from the interaction of solar energetic particles (SEPs) with the SEM detector (Jones, 2005; Private communication). Fig. 6(c) shows that on day 301, 2003 geomagnetic activity was very low, with DST > −44 nT.

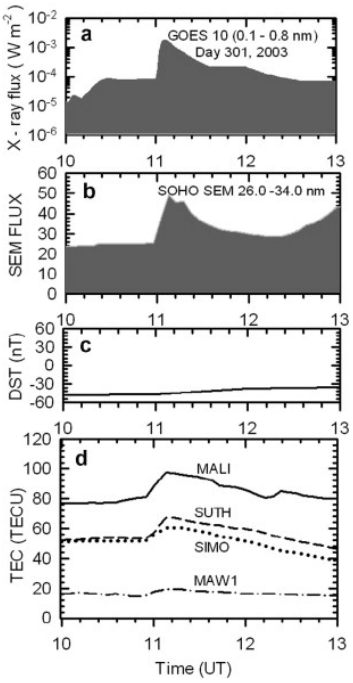

Fig. 6. The day 301, 2003 solar X17 flare. The different panels show: (a) GOES 10 five minute average X-ray fluxes on the 0.1–0.8 nm wavelength band, (b) SOHO SEM five minute average EUV fluxes on the 26.0–34.0 nm wavelength band, (c) Disturbance Storm Index (DST) measurements, and (d) UNB five minute TEC observed over MALI (solid line), SUTH (dashed line), SIMO (dotted line) and MAW1 (dash-dot-dash line) respectively. The SEM EUV fluxes are in units of (photons/cm^2/s × 10^9).

Fig. 6(d) shows the ionospheric TEC response to the day 301, 2001 flare event over GPS stations MALI (near equatorial), SUTH and SIMO (mid-latitude) and MAW1 (high latitude) respectively. A sudden rapid increase in TEC over all GPS stations is evident from ~11:00 UT to ~11:10 UT and decreases gradually to reach values comparable to the values before the flare onset at ~12:40 UT. In particular, during the first rapid phase of the flares TEC over these locations was enhanced with respect to the background (prior) values as follows: MALI by ~20 TECU, SUTH by ~16 TECU, SIMO by ~8 TECU, and MAW1 by ~4 TECU, respectively. It is evident from these results that TEC values were significantly enhanced for a near equatorial station (MALI), and the enhancement values decrease with increasing geographic latitudes of the GPS station to have lower values at MAW1. These results are consistent with Tsurutani et al. (2005) who reported that the largest TEC enhancement occurred at the sub-solar region (Africa equatorial GPS station), with TEC increase of ~22 TECU above the background. It is evident that the EUV flare associated with the X-ray flare causes photoionisation within the daytime ionosphere which results in significant TEC enhancements lasting longer (~3 h) than the duration of the flare.

Comparison of the two X-ray/EUV flares analyzed in this work indicates that the X28 flare was the largest and most intense in the 0.1–0.8 nm wavelength band, indicative of strong spectral variability between the two. The EUV flare event associated with this flare has a high intensity and a sharp peak. The high intensity (~90×10^9 photons/cm^2/s) sharp feature of the flare peak may lead to enhanced localized photoionisation within the daytime ionosphere. The latter possibility should be investigated in future work on the flare-ionosphere relationship. The EUV flare associated with the X17 flare has moderate intensity (~50×10^9 photons/cm^2/s) with a slightly broad peak. The broad sharp feature of this flare peak could be responsible for the global photoionisation within the daytime ionosphere. Further investigations on the characteristics of X-ray/EUV flares using more data sets is required to better understand their effects on the ionosphere.

4.2. Comparison of UNB TEC with IRI predictions

Fig. 7 compares daytime hourly average UNB (solid line) and IRI 2001 TEC (dashed line) computed for day 105, 2001 over (a) SUTH and (b) MAW1 GPS stations to test the reliability of the UNB results. TEC computed over SUTH for both models is comparable and increases significantly from 5:00 UT to reach maximum value of ~80 TECU at local noon (~10:00 UT), thereafter decreases gradually as expected. There is a very good correlation (r^2 = 0.984) between the two models over SUTH as shown in Fig. 7(c). For MAW1, TEC computed from both models increases gradually to reach a maximum value of ~32 TECU at ~10:00 UT and decreases after noon. However, there is an ~10 TECU difference between the UNB and IRI model results during the period ~10:00 UT to ~15:00 UT. A reason could be that the UNB underestimated TEC over the ocean because of a lack of data coverage. On the other hand, it could be that the IRI model is not accurate for predictions over southern Africa, where there is historically a lack of data coverage. As a result, a correlation coefficient of (r^2 = 0.673) between the two models over MAW1 was obtained as shown in Fig. 7(d). However, it is clear that in general both models show a good agreement during a geomagnetically quiet day at mid and higher latitudes. Future work includes validation of UNB TEC results using Ionosonde measurements over South Africa.

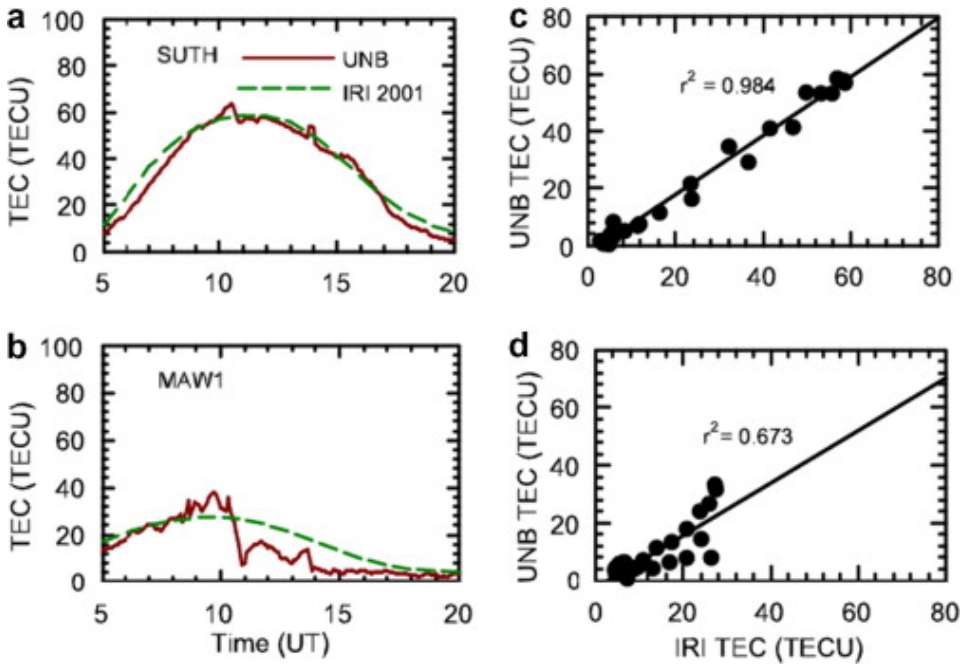

Fig. 7. Comparison of UNB (solid line) and IRI (dashed line) daytime TEC over the (a) SUTH and (b) MAW1 GPS stations for day 105, 2003. Panels (c) and (d) show the correlation coefficient computed by fitting a linear regression between UNB and IRI TEC over SUTH and MAW1 to provide an indication of the reliability of the UNB results.

5. Summary and conclusions

This paper reports on the current research effort being undertaken to study the solar cycle variations of GPS-derived TEC observed over southern Africa by applying the UNB ionospheric modelling technique. By using the sunspot number as a proxy for solar activity, TEC maps over South Africa were produced for day 345 at 14:00 UT during different epochs of solar cycle 23. It was found that the TEC values observed during extreme solar maximum conditions are significantly enhanced compared to the TEC values at different phases (epochs “a” and “c”) of the solar cycle observed during moderate solar activity conditions. The enhancement of TEC from moderate to extreme solar activity conditions is associated with the increased rate of production of background Solar X-ray and EUV radiation causing high rates of photoionisation within the daytime ionosphere. Of particular interest was the observed midlatitude peak display on the TEC map at extreme solar maximum, which was noteworthy for the enhanced ionisation at midlatitudes. An analysis of the geomagnetic storm activity index was performed in an attempt to investigate the causes of the observed TEC anomaly at midlatitudes. It was found that day 345, 2001 was geomagnetically quiet. A further investigation was conducted by analyzing the five minute average daytime GOES 8 satellite X-ray flux (0.1–0.8 nm) and SOHO SEM flux on 26.0–34.0 nm wavelengths. Comparison of these physical quantities revealed that there was a solar X-ray flare of magnitude X28 with an associated EUV flare event on day 345, 2001. Subsequent effects of these flares were investigated on the

daytime TEC observed over GPS stations MALI (near equatorial), SUTH, HARB, S121 (midlatitude) and MAW1 (high latitude) respectively. It was found that the EUV flare associated with the X28 flare seems to have caused significant TEC variations at midlatitudes, no such variations was evident at the lower and higher latitudes. The effects of this flare seem to be localized and the high TEC peak observed at midlatitudes may presumably be due to particle precipitation from the outer radiation belt at latitude >30° South that resulted from this flare. Although the latter explanation is likely, more data is required to substantiate this possibility.

Further investigations of solar flare effects on daytime TEC was pursued by selecting the X17 flare which occurred on the geomagnetically quiet day 301, 2003 over four GPS stations located at different latitudes. It was found that the EUV flare associated with this X-ray flare caused global photoionisation within the daytime ionosphere which led to a sudden increase of TEC which lasted longer than the duration of the flare. It was also evident that the TEC enhancement, with respect to the background values, was significantly higher at lower latitudes near the equatorial region and decreased towards the higher latitudes. This confirmed the TEC dependence on geographic locations and is consistent with the findings of Tsurutani et al. (2005).

A comparison of the EUV flares associated with the solar X28 and X17 flares analyzed in this work was performed. It was found that the EUV flare associated with X17 caused a global ionospheric effect in contrast to the localized midlatitudes ionospheric perturbations, which could be due to the EUV component of the X28 flare. A further investigation of the characteristics of EUV/X-ray flares and their relation to the ionosphere is required. A comparison of the daytime UNB and IRI 2001 models was performed to test the reliability of the UNB model results in reproducing the IRI 2001 predictions. It was found that the models show a good agreement during a geomagnetically quiet day at mid and higher latitudes. Future work will include a comparison with ground based ionospheric measurements to verify TEC computed with UNB code over South Africa.

Acknowledgements

The Space Geodesy Programme of the Hartebeesthoek Radio Astronomy Observatory (HartRAO) is grateful to Prof. Langley of Department of Geodesy and Geomatics Engineering, University of New Brunswick (UNB), Canada for providing us with a Unix-based FORTRAN code for the UNB ionospheric modelling technique for scientific research purposes. The author (DMM) would like to acknowledge the helpful discussions of the participants of the IRI 2005 Workshop organized by Ebre Observatory, Spain and Dr. N. Jakowski at the German Aerospace Center, Institute of Communication and Navigation, Neustrelitz. We are also grateful for the following institutes for providing online data to the international scientific community: International GNSS Service, South Africa CDSM Trignet, Solar Influence Data Analysis Center for the Sunspot Number, World Data Center for geomagnetism, University of Southern California Space Science Center for SOHO CELIAS/SEM data and National Geophysical Data Center at NOAA for GOES satellite solar X-ray flares data. The author is thankful to the South Africa National Research Foundation/HartRAO for financial support.

References

Bilitza, D. International Reference Ionosphere 2000. Radio Sci. 36, 261– 275, 2001.

Cilliers, P.J., Gouws, D., Opperman, B., Wonnacott, R.T., Combrinck, L. The southern African network of dual frequency global positioning system satellite receiver base stations: A national asset with many applications and research opportunities. S. Afr. J. Sci. 99, 51–55, 2003.

Combrink, A.Z.A., Combrinck, W.L., Moraal, H. Near real-time detection of atmospheric water vapour using the SADC GPS network. S. Afr. J. Sci. 100, 436–442, 2004.

Donnelly, R.F. Empirical models of solar flare X-ray and EUV emissions for use in studying the E and F region effects. J. Geophys. Res. 81, 4745, 1976.

Fedrizzi, M., Langley, R.B., Komjathy, A., Santos, M.C., de Paula., E.R. Kantor, I.J. The low-latitude Ionosphere: Monitoring its behaviour with GPS. in: Proceedings of ION GPS-2001, Salt lake City, Institute of Navigation, pp. 2468–2475, 2001.

Fedrizzi, M., de Paula, E.R., Kantor, I.J., Langley, R.B., Komjathy, A., Batista, I.S., Kantor, I.J. Study of the March 31, 2001 magnetic storm effects on the ionospheric GPS data. Adv. Space Res., 534–545, 2005.

Gail, W.B., Prag, A.B., Coco, D.S., Coker, C. A statistical characterization of local mid-latitude total electron content. J. Geophys. Res. 98, 15.717–15.727, 1993.

Hovestadt, D., Bochsler, P., Gru¨nwaldt, H., et al. CELIAS-charge, element, and isotope analysis system for SOHO. Sol. Phys. 162, 441–481, 1995.

Immel, T.J., Mende, S.B., Frey, H.U., Østgaard, N., Gladstone, G.R. Effect of the 14 July 2000 solar flare on Earth's FUV emissions. J. Geophys. Res. 108, 1155, 2003.

Jakowski, N. TEC monitoring by Using Satellite Positioning Systems, in: Kohl, H., Ru¨ ster, R., Schlegel, K. (Eds.), Modern Ionospheric Science. Max-Planck-Intitut fu¨ r Aeronomie, pp. 371–390, 1996.

Jakowski, N., Schlüter, S., Sardo´n, E. Total electron content of the ionosphere during the geomagnetic storm on 10 January 1997. J. Atmos. Sol. Terr. Phys. 61, 299–307, 1999.

Jakowski, N., Heise, S., Wehrenpfenning, S., et al. TEC Monitoring by GPS – A possible contribution to space weather monitoring. Phys. Chem. Earth (C) 26, 609–613, 2001.

Jakowski, N., Heise, S., Wehrenpfenning, S., Schlüter, S., Reimer, R. GPS/GLONASS-based TEC measurements as a contributor for space weather forecast. J. Atmos. Sol. Terr. Phys. 64, 729–735, 2002.

Jee, G., Schunk, R.W., Scherliess, L. Comparison of IRI-2001 with TOPEX TEC measurements. J. Atmos. Sol. Terr. Phys. 67, 365–380, 2005.

Jones, A.R. Space Sciences Center, University of Southern California, Los Angeles, Private communication, 2005.

Judge, D.L. First solar EUV irradiance obtained from SOHO by CELIAS/SEM. Sol. Phys. 177, 261, 1998.

Judge, D.L., McMullin, D.R., Gangopadhyay, P., et al. Space weather observations using SOHO CELIAS complement of instruments. J. Geophys. Res. 106, 29963–29968, 2001.

Judge, D.L., Ogawa, H.S., McMullin, D.R., Gangopadhyay, P., Pap, J.M. The SOHO CELIAS/SEM EUV database from SC23 minimum to the present. Adv. Space Res. 29, 1063–1968, 2002.

Klobuchar, J.A. Ionospheric effects on GPS. GPS World 2, 48–51, 1991.

Komjathy, A. Global Ionospheric Total Electron Content Mapping Using the Global Positioning System, Dept. of Geodesy and Geomatics Engineering, Technical Report No. 188, Ph.D. dissertation, University of New Brunswick, 1997.

Komjathy, A., Langley, R.B. An assessment of predicted and measured ionospheric total electron content using a regional GPS Network, in: The Proceedings of the National Technical Meeting of the Institute of Navigation, pp. 615–624, 1996.

Komjathy, A., Langley, R.B., Bilitza, D. Ingesting GPS-derived TEC data into International Reference Ionosphere for single frequency radar altimeter ionospheric delay corrections. Adv. Space Res. 22, 793–801, 1998.

Mannucci, A.J., Wilson, B.D., Edwards, C.D. A new method for monitoring the Earth's ionospheric total electron content using the GPS global network. in: Proceedings of the ION GPS-93, 6th International Technical Meeting of the Satellite division of the Institute of Navigation, Salt lake, Utah, USA, VII, pp. 1323-1332, 1993.

Mannucci, A.J., Wilson, B.D., Yuan, D.N., Ho, C.M., Lindqwister, U.J., Runge, T.F. A global mapping Technique for GPS-derived ionospheric total electron content measurements. Radio Sci. 33, 565–582, 1998.

Mannucci, A.J., Tsurutani, B.T., Iijima, B.A., Komjathy, A., Saito, A., Gronzalez, W.D., Guarnieri, F.L., Kozyra, J.U., Skoug, R. Dayside global ionospheric response to the major interplanetary events of October 29-30 ''Halloween Storms''. Geophys. Res. Lett. 32, L12S02, 2005.

Meggs, R.W., Mitchell, C.N. A study into the errors in vertical total electron content mapping using GPS data. Radio Sci. 41, RS1008, 2006.

Meggs, R.W., Mitchel, C.N., Spencer, S.J. A comparison of techniques for mapping total electron content ouver Europe using GPS signal. Radio Sci. 39, RS1S10, 2004.

Mitra, A.P. Ionospheric Effects of Solar Flares. Springer, New York, p. 294, 1974.

Ngcobo, S., Moeketsi, D.M., Combrink, A.Z.A., Combrinck, W.L. Ionospheric total electron content observed using the southern African GPS networks. S. Afr. J. Sci. 101, 537–539, 2005.

Ratcliffe, J.A. Magneto-ionic Theory and its Application to the Ionosphere. Cambridge University Press, Cambridge, 1959.

Skoug, R.M., Gosling, J.T., Steinberg, J.T., McComas, D.J., Smith, C.W., Ness, N.F., Hu, Q., Burlaga, L.F. Extremely high speed solar wind:29–30 October 2003. J. Geophys. Res. 109, A09102, 2004.

Smith, E.J., Marsden, R.G. Ulysses observations at solar maximum: Introduction. Geophys. Res. Lett. 30, 8027, 2003.

Thome, G.D., Wagner, L.S. Electron density enhancements in the E and F regions of the ionosphere during solar flares. J. Geophys. Res. 76, 6883, 1971.

Tsurutani, B.T., Judge, D.L., Guarnieri, F.L., et al. The October 28, 2003 extreme EUV solar flare and resultant extreme ionospheric effects: Comparison to other Hallowen events and the Bastille Day event. Geophys. Res. Lett. 32, L003S09, 2005.

Tsurutani, B.T., Mannucci, A.J., Iijima, B.A., et al. Global dayside ionospheric upliftment and enhancement associated with interplanetary electric fields. J. Geophys. Res. 109, A08302, 2004.

Zhang, D.H., Xiao, Z. Study of ionospheric response to the 4B flare on 28 October 2003 using International GPS Service network data. J. Geophys. Res. 110, A03307, 2005.